CHEMISTRY OF MATERIALS

pubs.acs.org/cm

Article

Ultrasmall HgTe Quantum Dots with Near-Unity Photoluminescent Quantum Yields in the Near and Shortwave Infrared

Belle Coffey, Elise Skytte, Tasnim Ahmed, Eugenia S. Vasileiadou, Eric Yu Lin, Ash Sueh Hua, Elijah Cook, Stephanie M. Tenney, Ellen M. Sletten, and Justin Ryan Caram*

Cite This: *Chem. Mater.* 2024, 36, 7561−7569

Read Online

ACCESS | Metrics & More | Article Recommendations | Supporting Information

ABSTRACT: We demonstrate a low-temperature synthesis of ultrasmall (<2 nm) HgTe quantum dots (QDs) with superlative optical properties in the near and shortwave infrared. The tunable cold-injection synthesis produces HgTe QDs ranging from 1.7 to 2.3 nm in diameter, with photoluminescence maxima ranging from 900 to 1180 nm and a full-width at half-maximum of ∼100 nm (∼130 meV). The synthesized quantum dots display high photoluminescence quantum yields (PLQY) ranging from 80 to 95% based on both relative and absolute methods. Furthermore, samples retain their high PLQY (∼60%) in the solid state, allowing for first-of-their-kind photoluminescence imaging and blinking studies of HgTe QDs. The facile synthesis allows for the isolation of small, photostable HgTe quantum dots, which can provide valuable insight into the extremes of quantum confinement.

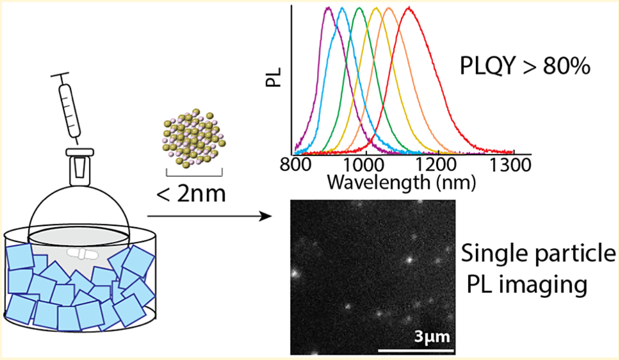

■ INTRODUCTION

Colloidal quantum dots (QDs) are nanometer sized crystals that display size dependent optical properties due to quantum confinement. Due to the semimetal/narrow bandgaps of bulk mercury chalcogenides and their concomitant large Bohr exciton radii (∼40 nm), HgX (X = S, Se, Te) nanocrystals display extreme bandgap tunability, from 1.5 eV to 20 meV (830 nm to 6.2 μm) for HgTe.[1−3] For this reason, HgX QDs are explored as low-cost solution processable alternatives for midwave infrared (3−5 μm) photodetection.[4,5] However, using HgTe QDs to explore short wave infrared (1 to 2 μm) imaging remains unexplored. There is great commercial interest in short wave infrared (SWIR) imaging due to the high spatiotemporal resolution for applications such as defense, noninvasive biomedical imaging, mobile devices, machine vision, advanced drive-assistance programs in cars, and more.[6−9] To date, most mercury chalcogenide QD research has focused on larger particles with optical bandgaps beyond the current detection range of commercial SWIR cameras (greater than 1600 nm).[10−13] Considerably less is known about the synthetic routes and optical properties of small (<3 nm) HgTe QDs, despite potential applications in near and shortwave infrared (NIR/SWIR) technologies such as SWIR imaging agents, photodetectors, light-emitting diodes, and other optoelectronic applications.[10−12,14−18]

In 2001, Rogach et al. reported HgTe nanocrystals with an excitonic absorbance feature at 830 nm (1.5 eV), photoluminesence spanning from 800 to 1400 nm and a photoluminescence quantum yield (PLQY) of 50%.[2] In 2021, Prado et al. observed a small HgTe cluster with an excitonic absorbance feature at 900 nm (1.37 meV).[14] Once isolated, the sample displayed an absorbance maxima of around 1100 nm (1.12 eV) and a PLQY of 75%. Similarly, 2 to 3 monolayer HgTe/HgSe nanoplatelets have been synthesized via cation exchange from cadmium chalcogenide materials availing extreme confinement and optical bandgaps from 600−885 nm (1.9−1.4 eV) and quantum yields from 10% to 56%.[19−22] However, in all these reports, despite high QYs, the fine-tuning of these nanomaterials in the near-infrared spectral window was not demonstrated.

Here, we present a novel "cold" injection approach to directly synthesize a series of ultrasmall (<2 nm) HgTe QDs with NIR/SWIR bandgaps. We estimate the size of these QDs through X-ray diffraction (XRD) and transmission electron microscopy (TEM) imaging to range from 1.72 to 2.39 nm in diameter. Interestingly, the ultrasmall s retain a high PLQY (40−80%) in a variety of polar and nonpolar solvents as well as in thin films. Comparative imaging on a SWIR InGaAs camera demonstrates their brightness in comparison to reference dye

Received: June 11, 2024
Revised: July 22, 2024
Accepted: July 23, 2024
Published: August 2, 2024

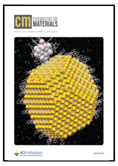

ACS Publications

https://doi.org/10.1021/acs.chemmater.4c01619

IR-1061. The solid-state stability of the QDs allows for the first single-particle photoluminescence imaging of HgTe QDs and the observation of photoluminescence intermittency (blinking) consistent with single QD resolution. Our results indicate that HgTe QDs can access the extreme confinement regimes and motivate the use of small HgTe QDs as candidates for high-efficiency emitters for NIR/SWIR device applications.

■ EXPERIMENTAL SECTION

Chemicals. Toxic mercury(II) acetate (99%) purchased from Sigma-Aldrich was used with extra care. All the chemicals were used as received from the manufacturer unless otherwise stated. The following solvents and reagents were purchased and used as recieved from Thermo-Fischer Scientific; *n*-trioctylphosphine (TOP), tetrachloroethylene (TCE), *n*-hexanes, acetone, ethanol, 2-propanol, dichloromethane (DCM), and methanol. Oleylamine (70%), Tellurium powder (99%), 1-dodecanethiol (DDT), and infrared dyes IR-140 and IR-1061 were purchased from Sigma-Aldrich.

TOPTe Preparation. TOPTe was prepared in a glovebox at room temperature according to the published procedure.[23] A stock solution of 1.0 M TOPTe was prepared by dissolving tellurium powder (250 mg) in *n*-trioctylphosphine (2 mL) inside the glovebox. The Te/TOP solution was allowed to stir overnight to form a clear yellow solution. The 1.0 M stock solution was diluted to 0.50 M with tetrachloroethylene for the QD synthesis.

Synthetic Procedure of the "Cold" Injection HgTe QDs. The reaction is performed under ambient atmosphere. Mercury(II) acetate (0.150 g, 471 μmol) is dissolved in 6 mL of oleylamine (70%). Light heat is applied to the stirring solution until all the mercury salt has dissolved. Once the mercury has dissolved, the solution is allowed to cool to room temperature. The reaction flask is placed in an ice bath and cooled to approximately 6 °C. The tellurium source solution is then injected into the reaction flask, causing an immediate color change to brown. The injected tellurium source solution contains 0.50 M TOPTe (0.250 mL, 125 μmol) and dodecanethiol (10 μL of a 20 mM DDT solution in TCE, 0.2 μmol). The reaction is allowed to react in the ice bath (~5 min), then removed and allowed to stir at room temperature for the remainder of the reaction. Aliquots of the solution are removed to probe the reaction via absorbance measurements where the appearance and shift of an excitonic feature is monitored.

If the reaction is fully cooled in an ice bath (~6 °C), an excitonic feature at 715 nm is observed almost immediately after injection. The observed absorbance features shift continuously for approximately 1 h. The size and optical properties of the QD can be tuned by the reaction length before quenching. The reaction is quenched with a 20 mM DDT solution in TCE (4 mL, 80 μmol). The quenched product is then isolated through centrifuging with a 1:1 ratio of 2-propanol at 12,500 rpm for 3:00 min. The isolated powder is washed once with 2 mL of 2-propanol and dissolved into 5 mL of TCE. The isolated product is stored overnight in the freezer to increase stability. If the samples are left out at room temperature for more than 24 h, ripening is observed along with a decrease in PLQY.

Photophysical Characterization. All the samples used for optical characterization were concentrated at an optical density (O.D.) of 0.10 or less. Absorption spectra were recorded with an Agilent Cary 60 UV−vis spectrophotometer. Photoluminescence spectra were measured with a Horiba Scientific PTI QuantaMaster400 spectrometer equipped with liquid nitrogen-cooled InGaAs photodiode and Si photomultiplier tube detectors. Absolute photoluminescence quantum yield (PLQY) measurements were recorded with a petite integrating sphere on the Horiba spectrometer. Infrared emitting dyes IR-140 ($Q_f = 0.167$)[24] and IR-1061 ($Q_f = 5.0 \times 10^{-3}$)[25] were used as references for the relative quantum yield measurements. Photoluminescent lifetime measurements were performed on a home-built optical set up, using short-wave sensing superconducting nanowire single photon detectors (SNSPDs) and a time-lagged single-photon counting module.[26] For lifetime measurements, a 405 nm laser at a 1 MHz repetition rate was used.

■ RESULTS AND DISCUSSION

We described the synthetic procedure in detail in the experimental section. Our method differs from prior approaches to isolating small HgTe QDs in several ways. First, we utilize low temperatures (<10 °C compared to 25−100 °C)[14,23] to suitably slow the reaction and access early time kinetics of these nanoclusters.[14,23] Lower temperatures necessitate the use of mercury(II) acetate as the precursor salt, which has a higher solubility in oleylamine in contrast to other common mercury halide salt precursors. Finally, we add a small amount of 1-dodecanethiol (DDT) into our tellurium source solution. The S−Hg bond of dodecanethiol is known to be strong, which enables strong surface passivation and decreased aggregation in the nucleation phase of HgTe QD growth.[27,28]

In a typical synthesis, mercury(II) acetate is dissolved into excess oleylamine and held in a water ice bath. A solution containing tellurium dissolved in trioctylphosphine (TOPTe) and DDT is injected into the cooled reaction mixture, upon which the solution turns brown. Aliquots of the reaction are extracted and probed using UV−vis spectroscopy over 1 h. The reaction is quenched with a solution of excess dodecanethiol diluted in TCE resulting in well-suspended QDs capped with DDT. We then centrifuged the product and redissolved the QDs in TCE for optical characterization. The rate of reaction, size, and optical properties of the synthesized HgTe QDs can be tuned based on the temperature of the Hg/oleylamine solution in the ice bath before TOPTe injection or the reaction length before quenching. In Figure 1a, we show the absorbance and photoluminescence spectra of QD samples synthesized under the same conditions (6 °C injection) and differ only in the reaction time. After approximately 1 h, no further shifts in the absorbance spectrum are observed suggesting that the tellurium source is consumed. Therefore, from nucleation the excitonic absorbance feature can be tuned around 250 nm. The surface passivation and atomic percentage of the QDs was analyzed using energy dispersive spectroscopy (EDS). The EDS confirms the HgTe identity of the QDs, and that they are passivated with DDT (S1).

When the reaction is quenched immediately after TOPTe injection, a strong excitonic feature is observed in the absorbance spectrum at 715 nm (1.73 eV) (Figure 1a). This represents the lowest absorbance wavelength and smallest particles produced via this synthetic method. We also compare absorbance features of small HgTe QDs nearest to ours in size from the literature as seen in Figure 1b, demonstrating the difference in the band gaps. To the best of our knowledge there are only two reports of HgTe QDs with absorbance features at 900 nm or below, which still exhibit red-shifted absorbance features (830 nm, 900 nm) and PL maxima (1050 nm, 1200 nm) than our smallest sample with absorbance at 715 nm and PL maxima at 915 nm. (Figure 1a,b).[2,14]

Throughout the course of one reaction, the PL maxima can be tuned to ~200 nm. A fully cooled reaction flask will produce QDs with PL maxima ranging from 915 to 1100 nm (Figure 1a). When the reaction flask is not allowed to fully cool, the reaction can be extended to isolate QDs with PL maxima up to ~1200 nm (Figure S2). The QD samples show relatively narrow full-width at half-maximum (FWHM) of their photoluminescence spectra ranging from 100 to 154 nm (130−140 meV) for the smallest to largest QDs sampled, which is consistent or prior reports of the FWHM for HgTe

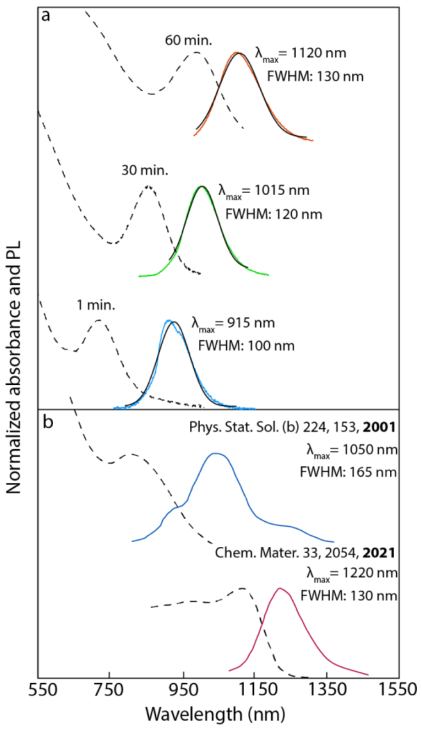

Figure 1. (a) Absorbance and photoluminescence (PL) spectra of the solution samples isolated from a standard cold injection reaction performed at 6 °C. All the spectra were recorded in TCE. Absorbance spectra are denoted in black dashed lines, while PL is shown in solid color. The reaction length of each sample is denoted, and the Gaussian fit used to extract the FWHM is shown over the PL spectra. The λ_{max} and FWHM of each PL spectra is denoted. (b) Absorbance and PL spectra of HgTe QDs most similar in size and photophysical properties from literature.[2,14] The λ_{max} and FWHM of each PL spectrum is denoted. Spectra reproduced with permission from ref 2. (Copyright 2001 Wiley) and[14] (Copyright 2021 American Chemical Society).

QDs of similar photoluminescence wavelengths; 130 nm (110 meV),[14] 195 nm (190 meV).[2] In a standard reaction, the FWHM broadens (100 to 134 nm) as a function of reaction time (Figure 1a). The increase in the FWHM as the reaction progresses over long reaction times provide an early suggestion that an Ostwald ripening mechanism may be responsible for the growth of the QDs.[29] Similar FWHM behavior and reaction kinetics were observed in a single injection synthesis of InAs QDs, attributed to an Ostwald ripening mechanism of growth.[13]

To estimate the size of the ultrasmall HgTe QDs, we used powder X-ray diffraction (PXRD) measurements and TEM imaging. TEM sizing analysis was performed on the smallest and largest samples from the synthesis, and was found to be 1.65 and 2.29 nm (±0.30 nm), respectively (Figure 2a). Sizing distributions collected from TEM analysis were plotted, and the histograms were fit to a Gaussian function (Figures 2b, S3). The sizing distributions have a standard deviation for the smallest QD sample (1.65 nm) of 0.28 nm and 0.36 nm for the larger QDs (2.29 nm) imaged. We performed PXRD on five zinc blende HgTe QDs and used the Scherrer equation to estimate particle diameter (S4).[30] The (111) reflection was fit to a Gaussian equation to extract the FWHM for the Scherrer equation (Figure 2c). The analyzed samples were found to range in size from 1.72 to 2.29 nm (±0.30 nm).[31] The PXRD results were corroborated with TEM imaging (Figure 2b,c). TEM sizing analysis was performed on the smallest and largest samples from the synthesis which were found to be 1.64 and 2.40 nm (±0.30 nm) respectively (Figure 2c). Our samples follow a consistent trend when the absorbance feature is plotted as a function of particle diameter, as shown in the sizing curve presented (Figure 2d). The sizing curve focuses on HgTe QDs with interband transitions of 10 μm or less (or under 20 nm in diameter), where the data points and fits were gathered from various references.[3,12,14,27,32−36] Current fits for the HgTe QD sizing curve are prove to be outdated and break down as the synthetic scaffold of sizes continues to expand

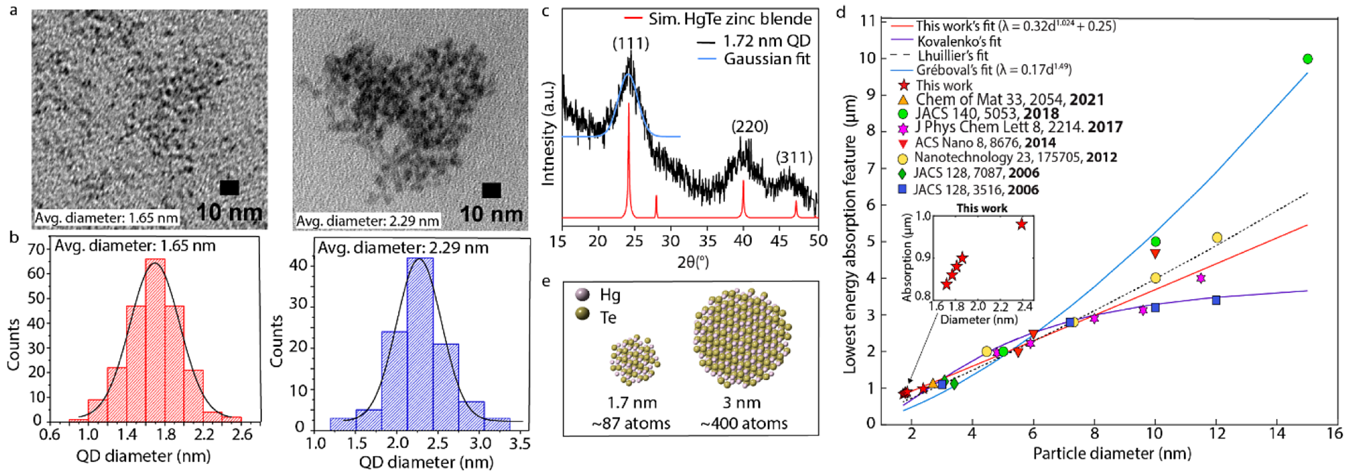

Figure 2. (a) TEM images of QDs used for sizing analysis. The left image shows the smallest sample size (1.65 nm) and the largest sample size (2.29 nm). (b) The corresponding sizing distribution histogram from the TEM image. The histogram for the smallest QD sampled (1.65 nm) is shown on the left in red, where the largest QD sampled is shown on the right in blue (2.29 nm). Both histograms are fit to a Gaussian function shown in black. The statistics of the sizing distributions can be found in the Supporting Information (S3). (c) PXRD pattern of a HgTe QD sized to be 1.72 nm via Scherrer analysis. Diagnostic zinc blende reflections are labeled. The simulated HgTe zinc blende pattern is included. (d) Sizing curve extracted from the related references and empirical fit from literature. The plot features the absorbance of characterized HgTe QDs from literature as a function of particle diameter. Our data points are plotted in the inset. (e) Crystal maker graphics of a 1.7 nm zinc blende HgTe QD (~87 atoms) and a 3 nm HgTe QD (~400 atoms).

https://doi.org/10.1021/acs.chemmater.4c01619
Chem. Mater. 2024, 36, 7561−7569

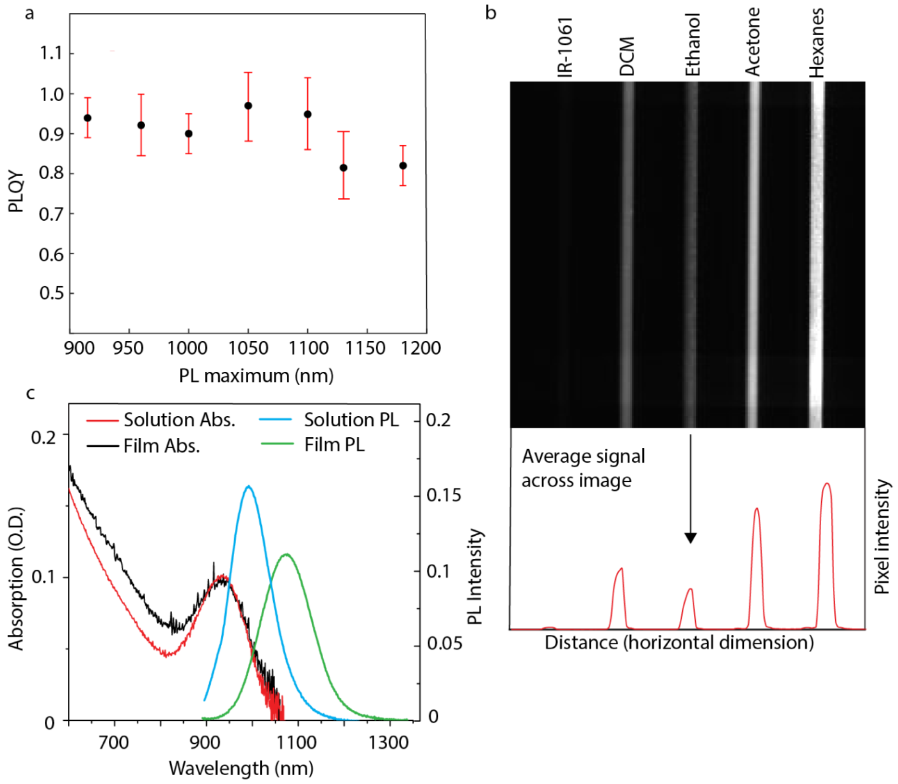

Figure 3. (a) Photoluminescence quantum yield (PLQY) plotted as a function of PL maxima. Reference dyes IR-1061[25] and IR-140[24] were used to measure the PLQY via relative methods (S5). (b) Capillary image of a HgTe QDs dissolved in various solvents and concentration matched at the excitation wavelength of 890 nm. The samples were uniformly excited and imaged alongside one another to compare the relative brightness in each solvent. A reference dye IR-1061 ($QY = 5 \times 10^{-3}$)[25] was included for qualitative comparison. A rectangular ROI was drawn over the relevant area of the raw image and used to crop the images to the displayed size. The average signal intensity is plotted as a function of horizontal distance and is shown below. Camera settings were as follows: gain = 1, ET = 0.1 ms. (c) PL and absorbance of HgTe QD sample thin film and in solution dissolved in TCE. The solution and film sample were concentration matched to the excitation wavelength of 890 nm. The raw PL intensity of the thin film sample (blue) and solution state (green) sample are plotted along with the absorption from each sample.

(Figure 2d). Our data collected from the PXRD are included and plotted in the inset (Figure 2d). Our calculated sizes align well with the trend, though we are able to sample a much smaller range of sizes (down to ∼1.7 nm) than those previously isolated (∼3 nm).[14,33,36] For context, 2.7 nm QDs (reported by Prado et al.[14]) contain ∼400 atoms, whereas 1.7 nm samples contain ∼90 atoms (Figure 2e). The small size of our ∼90 atom QDs is similar in scale to the magic size clusters isolated in Cd chalcogenide syntheses.[37−41]

The small HgTe QDs are colloidally stable and display a bright photoluminescence. Photoluminescent quantum yields (PLQY) were evaluated using both an integrating sphere (absolute) and via comparison to known standards (relative) (S5). With little optimization, PLQYs were above 80% for all samples, and near unity for the NIR QDs (Figure 3a) in TCE. Our results confirm prior reports of high QY (>50%) in small HgX QDs.[2,14,15] Furthermore, excited-state photoluminescence decay measurements were performed on representative HgTe QD samples (S6). Upon 405 nm pulsed excitation, the QDs show a nearly monoexponential lifetime of ∼7 ns (Figure S8). The primary lifetime of 7 ns is consistent with the lifetimes observed for the excitonic transitions in HgTe QDs (2 ns)[42] and highly confined 2 to 3 monolayer HgTe nanoplatelets (7−50 ns).[19,20]

We then investigated the photoluminescence of HgTe QDs in a variety of organic solvents such as hexanes, acetone, dichloromethane, and ethanol. A stock HgTe QD solution was diluted to have the same optical density at the excitation source wavelength of 890 nm in each of the solvents tested. To compare the brightness of the photoluminescence, the samples were uniformly excited with 890 nm light and imaged with a SWIR camera alongside one another (S7). A reference dye IR-1061 with a known PLQY was also included in a capillary tube in the image for comparison.[25] The QD photoluminescence is the brightest and most stable in hexanes, followed by acetone, DCM, and ethanol (Figure 3b). To demonstrate the relative brightness of the sample in each solvent, the pixel intensity across the image was plotted (Figure 3b). Compared to the bright HgTe QD samples, the dye has very little pixel intensity, which is consistent with the low QY of IR-1061 of 5.0×10^{-3}.[25] The trend in the relative brightness was corroborated through quantum yield measurements in each of the tested solvents (S8). The sample had the highest PLQY in TCE (90%) calculated with IR-1061 as the reference dye. The PLQY results for each studied solvent corroborated the trend observed in the SWIR images. The QY remains the highest in hexanes (83%), followed by acetone (66%) and DCM (56%), and wad found to be the lowest in ethanol (36%). Although these samples are highly emissive in polar solvents, such as ethanol, the photostability of the QDs decreases over hours in such solvents. Future work will focus on surface ligand modification to improve polar solvent solubility and long-term photostability.

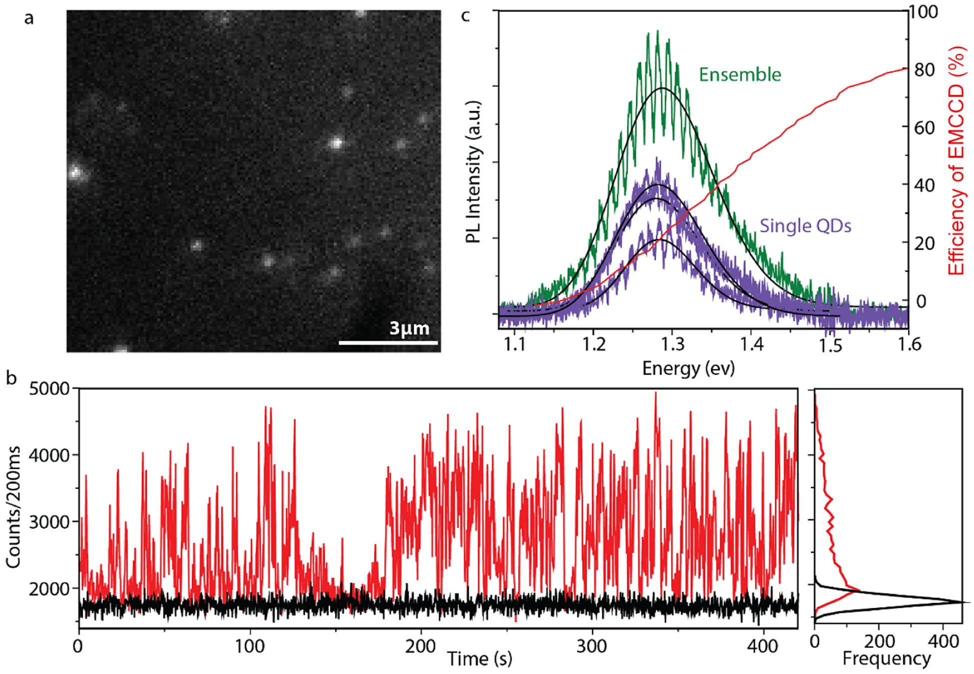

Figure 4. (a) Photoluminescence (PL) microscopy image of thin film of QDs at room temperature obtained using a wide-field fluorescence microscope (S10). (b) PL intensity time-trace (red) of a single QD and the background (black). The background trace is recorded from an area on the film where no particles existed. The right panel shows the frequency of the PL intensity trace of QD. (c) The PL spectra of three single QDs and the ensemble film. The detector efficiency is plotted over the PL traces to show the low efficiency PL region of interest.

The small HgTe QDs retain their photoluminescence properties in the solid state. The solid-state photoluminescence was investigated in thin films. A representative QD sample was concentrated to match the optical density of a drop-cast thin film (Figure 3c). The representative QD sample used in the comparative experiment has a relatively small Stokes shift in the solution (~50 nm). The Stokes shift can vary between samples likely due to a larger distribution of sizes in some samples. For example, a sample of similar PL wavelengths shown in Figure 1a has a larger Stokes shift (~100 nm) in comparison to the representative sample from Figure 3c (~50 nm). We compared the relative photoluminescence intensity and spectra of the representative sample in film and solution. The film retains the majority of the photoluminescence intensity that the solution sample has. In thin film, a red shift in the photoluminescence maximum (from 1050 to 1100 nm) and broadening of the FWHM (by 40 nm) are observed (Figure 3c). The red shift in photoluminescence observed in the solid state may be due to energy transfer occurring, film inhomogeneity, or reabsorption.[21,42] To estimate the relative quantum yield of the film, the ratio of the optical density and integrated PL intensity in solution and film were compared. The solution QD sample in TCE was found to have a PLQY of ~80% through absolute and relative methods. By comparing the ratio of the absorbance O.D. and integrated photoluminescence spectra of the QDs in film and solution, we estimated the PLQY of the film to be ~60%. We then imaged the photoluminescence of solid HgTe QDs on a SWIR InGaS camera in the same method as described previously (S7). The HgTe powders display bright photoluminesence on the SWIR camera (S9), which is significant as the photoluminesence of QDs can commonly quench in the solid state.[42−44] However, our QD samples can retain strong solid-state photoluminescence and ~60% quantum yields in thin films.

The photostability of the QDs in thin films allowed us to study the photoluminescence spectra and intermittency under a fluorescence microscope with single particle resolution. The photoluminescence dynamics of other infrared nanocrystals, PbS and InAs QDs, have been investigated at the single particle level.[45−51] However, no single particle study has been performed on HgTe QDs before. A home-built wide-field photoluminescence microscope was utilized to study the single particle photoluminescence of the ultrasmall HgTe QDs (S10). The thin films used for single particle imaging were prepared by drop casting a diluted hexanes solution of QDs onto a glass coverslip at a small incline. The film was excited by a 405 nm continuous wave diode laser with an intensity of 200 W/cm^2. The photoluminescence of the film was recorded over time using an EMCCD camera. It is noteworthy that in our case the efficiency of the camera is <20% in the spectral region of interest (~950 nm). The low camera efficiency in this region makes it challenging to record any photoluminescence, however the high PLQY and brightness enables imaging of the QDs at single particle resolution.

The thin films used for single-particle imaging were well dispersed with bright QDs, as shown in the photoluminescent images and video (Figure 4a and Video S1). We analyzed the photoluminescence intensity traces of 50 individual QDs. All the single QDs sampled display photoluminescence intermittency (blinking), where discrete periods of no photoluminescence intensity (or off states) are observed (Figure 4b and Video S1). It is important to note that at a 405 nm excitation, the thin films exhibit a lower quantum yield (by ~20%), which likely increases the amount of blinking observed. The blinking behavior is similar to that observed universally for other types of nanocrystals.[46,48,51] Blinking in nanocrystalline systems is often attributed to a range of possible phenomena, including Auger recombination in charged QDs and nonradiative channels related to traps or hot-carrier trapping.[46,52−57] Power law analysis was performed on a plot of the on/off times of the single QDs sampled (S11). The on/off times show statistical power law distributions consistent with the dispersive kinetics, which could be due to possible charge trapping and detrapping in the QDs.

Despite observed blinking, the QDs were photostable under 405 nm excitation for longer than 6 min. The photoluminescence spectra of 10 single HgTe QDs were analyzed and compared with that of the ensemble film (Figure 4c). All single QD spectra analyzed have a FWHM narrower than the FWHM of the ensemble film. For single QDs sampled, the FWHM ranges from 103 to 125 meV, whereas the ensemble spectrum has a FWHM of 150 meV. Since the single QD FWHM values are narrower than the ensemble, this indicates some amount of inhomogeneous broadening in the ensemble spectra and room for improvement in the synthesis. However, we note that these are approximate values, as the camera efficiency declines precipitously above 900 nm. The single QD and ensemble photoluminescence FWHM observed are similar to those observed for other HgTe QD syntheses (110 meV, 195 meV)[2,14] and PbS QDs (~100 meV in the NIR).[46,47,50]

CONCLUSION

There are several nanocrystal systems that have optical transitions in the near and shortwave infrared. Lead chalcogenides can be quantum confined to emit from 1.5 to 0.3 eV (830 to 4000 nm), and have reported quantum yields in solution ranging from 3 to 90% strongly depending on the optical bandgap, but are limited by the bulk bandgaps (e.g., PbTe bandgap of 0.32 eV).[58−65] InAs and InSb also display size tunable SWIR bandgaps, ranging from 1.7 to 0.3 eV (730 to 4000 nm) with quantum yields of 2−82%, again variable and depending on shelling procedures.[13,29,66−68] However, HgTe appears to have some unique properties. First, as demonstrated in this manuscript, HgTe QDs display high quantum yields, which are air-stable without a core−shell procedure unlike the aforementioned indium and lead materials, which require shells to obtain high PLQY.[13,69] Second, HgTe QDs appear to show rather short radiative lifetimes (2−10 ns) consistent with other II−VI materials, but considerably shorter than Pb chalcogenides (>1 μs).[42,70,71] Third, HgTe QDs can be synthesized in air, and appear to be resistant against oxidative damage, unlike lead and indium-based nanomaterials.[14] Finally, as HgTe materials have no bulk bandgap, they can be quantum confined for long wave infrared (8−12 μm) to NIR/SWIR bandgaps.[11,32] Insight into the synthesis and properties is thus very widely applicable to next-generation sensor and camera technologies.

Nonetheless, we acknowledge the potential disadvantages of HgTe nanocrystals. First, Hg is a highly toxic metal, and the mercury salts used for HgTe syntheses are known to be acutely toxic if ingested or inhaled and corrosive to skin, so they must be handled with care.[72] Second, since HgTe QDs form at relatively low temperatures (0−100 °C), the as-synthesized stability has not been established at elevated temperatures. The low-temperature syntheses result in QDs, which are non-spherical and approaches to improve monodispersity remain a challenge.[23,73,74] Finally, we lack much fundamental insight into their underlying spectroscopic and physical properties in comparison to other II−VI, IV−VI, and III−V materials.[75−77] However, the superlative PLQY (>80%) of core-only HgTe QDs, the short lifetimes, and relative synthetic ease suggest future work may address these challenges.

Indeed, in our current manuscript, we utilize mercury acetate, which has proven to be less toxic and corrosive than the more common halogen precursor salt, mercury chloride.[78] Both mercury acetate and mercury chloride can form toxic fumes upon heating; therefore, by utilizing low temperatures, our synthesis reduces the risk of forming excess fumes.[79,80] Additionally, low temperatures may mitigate the formation of dangerous organomercury products, similar to cadmium chalcogenides, where organocadmium byproducts are suggested as short-lived intermediates during high-temperature cadmium chalcogenide QD syntheses.[81]

We demonstrate a tunable low-temperature synthesis for the direct isolation of a variety of HgTe QDs under 2 nm in size. Using a cold-injection synthesis, we produced a size series that maintains high PLQY and solid-state photoluminescence. The smallest of these samples represent clusters of roughly 90 atoms or less. Due to the excellent photoluminescence properties, the first single-particle photoluminescence imaging study on HgTe QDs was also performed. Overall, the presented cold injection synthesis provides an interesting platform to investigate the initial stages of HgTe nucleation and the smallest bounds of confinement for bulk HgTe. The efficient PLQY (>80%) and bright solid-state photoluminescence of the presented QDs motivate the use of small (<3 nm) HgTe QDs as emitters in NIR/SWIR devices.

ASSOCIATED CONTENT

Supporting Information

The Supporting Information is available free of charge at https://pubs.acs.org/doi/10.1021/acs.chemmater.4c01619.

Additional characterization and experimental methods, including PL spectra, EDS, XRD, relative PLQY methods, photoluminescence lifetimes, SWIR camera imaging methods, photoluminescence imaging methods, and power law analysis (PDF)

Video footage of intermittent photoluminescence of single QDs (AVI)

AUTHOR INFORMATION

Corresponding Author

Justin Ryan Caram − *Department of Chemistry and Biochemistry, University of California, Los Angeles, Los Angeles 90095-1569 California, United States;* orcid.org/0000-0001-5126-3829; Email: jcaram@chem.ucla.edu

Authors

Belle Coffey − *Department of Chemistry and Biochemistry, University of California, Los Angeles, Los Angeles 90095-1569 California, United States;* orcid.org/0000-0003-4347-5797

Elise Skytte − *Department of Chemistry and Biochemistry, University of California, Los Angeles, Los Angeles 90095-1569 California, United States*

Tasnim Ahmed − *Department of Chemistry and Biochemistry, University of California, Los Angeles, Los Angeles 90095-1569 California, United States*

Eugenia S. Vasileiadou − *Department of Chemistry and Biochemistry, University of California, Los Angeles, Los Angeles 90095-1569 California, United States*

Eric Yu Lin − *Department of Chemistry and Biochemistry, University of California, Los Angeles, Los Angeles 90095-1569 California, United States*

Ash Sueh Hua – *Department of Chemistry and Biochemistry, University of California, Los Angeles, Los Angeles 90095-1569 California, United States*

Elijah Cook – *Department of Chemistry and Biochemistry, University of California, Los Angeles, Los Angeles 90095-1569 California, United States*

Stephanie M. Tenney – *Department of Chemistry and Biochemistry, University of California, Los Angeles, Los Angeles 90095-1569 California, United States*

Ellen M. Sletten – *Department of Chemistry and Biochemistry, University of California, Los Angeles, Los Angeles 90095-1569 California, United States*; orcid.org/0000-0002-0049-7278

Complete contact information is available at:
https://pubs.acs.org/10.1021/acs.chemmater.4c01619

Author Contributions

B.C. synthesized and characterized all the materials along with the help from E.S. Single-particle photoluminescence imaging was done by T.A., PXRD was done by E.S.V, SWIR capillary imaging was done by E.Y.U, and photoluminescent lifetimes were collected by A.S.H. E.C assisted with TEM imaging and crystal maker graphics.

Notes

The authors declare no competing financial interest.

■ ACKNOWLEDGMENTS

The authors thank the Materials Characterization Laboratory at the University of California, Los Angeles (UCLA), for instrumentation. The authors acknowledge the use of instruments at the Electron Imaging Center for NanoMachines, supported by the National Institute of Health (1S10RR23057 to Z.H.Z.), and CNSI at UCLA. Funding support was given by the National Science Foundation under grant 1945572 and the Dreyfus Foundation under grant TC-22–087. We acknowledge funding for T.A. from the UC Office of the President within the Multicampus Research Programs and Initiatives (No. M23PR5931).

■ REFERENCES

(1) Rinnerbauer, V.; Hingerl, K.; Kovalenko, M.; Heiss, W. Effect of Quantum Confinement on Higher Transitions in HgTe Nanocrystals. *Appl. Phys. Lett.* **2006**, *89*, 193114.

(2) Rogach, A. L.; Harrison, M. T.; Kershaw, S. V.; Kornowski, A.; Burt, M. G.; Eychmüller, A.; Weller, H. Colloidally Prepared CdHgTe and HgTe Quantum Dots with Strong Near-Infrared Luminescence. *Phys. Status Solidi B* **2001**, *224*, 153–158.

(3) Goubet, N.; Jagtap, A.; Livache, C.; Martinez, B.; Portalès, H.; Xu, X. Z.; Lobo, R. P. S. M.; Dubertret, B.; Lhuillier, E. Terahertz HgTe Nanocrystals: Beyond Confinement. *J. Am. Chem. Soc.* **2018**, *140*, 5033–5036.

(4) Rogalski, A. Infrared Detectors: An Overview. *Infrared Phys. Technol.* **2002**, *43*, 187–210.

(5) Rogalski, A.; Antoszewski, J.; Faraone, L. Third-Generation Infrared Photodetector Arrays. *J. Appl. Phys.* **2009**, *105*, 091101.

(6) Hong, G.; Antaris, A. L.; Dai, H. Near-Infrared Fluorophores for Biomedical Imaging. *Nat. Biomed. Eng.* **2017**, *1*, 0010.

(7) Steckel, J. S.; Josse, E.; Pattantyus-Abraham, A. G.; Bidaud, M.; Mortini, B.; Bilgen, H.; Arnaud, O.; Allegret-Maret, S.; Saguin, F.; Mazet, L.; Lhostis, S.; et al. 1.62 μm Global Shutter Quantum Dot Image Sensor Optimized for Near and Shortwave Infrared. *2021 IEEE International Electron Devices Meeting (IEDM) IEEE* **2021**, 23–24.

(8) Steckel, J. S.; Pattantyus-Abraham, A. G.; Josse, E.; Mazaleyrat, E.; Rochereau, K. High Resolution Quantum Dot Global Shutter Imagers. *SID Symp. Dig. Tech. Pap.* **2021**, *52*, 975–977.

(9) Hong, G.; Diao, S.; Chang, J.; Antaris, A. L.; Chen, C.; Zhang, B.; Zhao, S.; Atochin, D. N.; Huang, P. L.; Andreasson.; et al. Through-Skull Fluorescence Imaging of the Brain in a New near-Infrared Window. *Nat. Photonics* **2014**, *8*, 723–730.

(10) Böberl, M.; Kovalenko, M. V.; Gamerith, S.; List, E. J. W.; Heiss, W. Inkjet-Printed Nanocrystal Photodetectors Operating up to 3 Mm Wavelengths. *Adv. Mater.* **2007**, *19*, 3574–3578.

(11) Keuleyan, S.; Lhuillier, E.; Brajuskovic, V.; Guyot-Sionnest, P. Mid-Infrared HgTe Colloidal Quantum Dot Photodetectors. *Nat. Photonics* **2011**, *5*, 489–493.

(12) Gréboval, C.; Chu, A.; Goubet, N.; Livache, C.; Ithurria, S.; Lhuillier, E. Mercury Chalcogenide Quantum Dots: Material Perspective for Device Integration. *Chem. Rev.* **2021**, *121*, 3627–3700.

(13) Franke, D.; Harris, D. K.; Chen, O.; Bruns, O. T.; Carr, J. A.; Wilson, M. W. B.; Bawendi, M. G. Continuous Injection Synthesis of Indium Arsenide Quantum Dots Emissive in the Short-Wavelength Infrared. *Nat. Commum.* **2016**, *7*, 12749.

(14) Prado, Y.; Qu, J.; Gréboval, C.; Dabard, C.; Rastogi, P.; Chu, A.; Khalili, A.; Xu, X. Z.; Delerue, C.; Ithurria, S.; et al. Seeded Growth of HgTe Nanocrystals for Shape Control and Their Use in Narrow Infrared Electroluminescence. *Chem. Mater.* **2021**, *33*, 2054–2061.

(15) Lee, G.; Jeong, W. H.; Kim, B.; Jeon, S.; Smith, A. M.; Seo, J.; Suzuki, K.; Kim, J.; Lee, H.; Choi, H.; Chung, D. S.; et al. Design and Synthesis of CdHgSe/HgS/CdZnS Core/Multi-Shell Quantum Dots Exhibiting High-Quantum-Yield Tissue-Penetrating Shortwave Infrared Luminescence. *Small* **2023**, *19*, 2301161.

(16) Geiregat, P.; Houtepen, A. J.; Sagar, L. K.; Infante, I.; Zapata, F.; Grigel, V.; Allan, G.; Delerue, C.; Van Thourhout, D.; Hens, Z. Continuous-Wave Infrared Optical Gain and Amplified Spontaneous Emission at Ultralow Threshold by Colloidal HgTe Quantum Dots. *Nat. Mater.* **2018**, *17*, 35–42.

(17) Qu, J.; Rastogi, P.; Gréboval, C.; Lagarde, D.; Chu, A.; Dabard, C.; Khalili, A.; Cruguel, H.; Robert, C.; Xu, X. Z.; et al. Electroluminescence from HgTe Nanocrystals and Its Use for Active Imaging. *Nano Lett.* **2020**, *20*, 6185–6190.

(18) Chen, H.; Li, L.; Cui, S.; Mahounga, D.; Zhang, J.; Gu, Y. Folate Conjugated CdHgTe Quantum Dots with High Targeting Affinity and Sensitivity for In Vivo Early Tumor Diagnosis. *J. Fluoresc.* **2011**, *21*, 793–801.

(19) Izquierdo, E.; Robin, A.; Keuleyan, S.; Lequeux, N.; Lhuillier, E.; Ithurria, S. Strongly Confined HgTe 2D Nanoplatelets as Narrow Near-Infrared Emitters. *J. Am. Chem. Soc.* **2016**, *138*, 10496–10501.

(20) Tenney, S. M.; Vilchez, V.; Sonnleitner, M. L.; Huang, C.; Friedman, H. C.; Shin, A. J.; Atallah, T. L.; Deshmukh, A. P.; Ithurria, S.; Caram, J. R. Mercury Chalcogenide Nanoplatelet–Quantum Dot Heterostructures as a New Class of Continuously Tunable Bright Shortwave Infrared Emitters. *J. Phys. Chem. Lett.* **2020**, *11*, 3473–3480.

(21) Tenney, S. M.; Tan, L. A.; Tan, X.; Sonnleitner, M. L.; Coffey, B.; Williams, J. A.; Ronquillo, R.; Atallah, T. L.; Ahmed, T.; Caram, J. R. Efficient 2D to 0D Energy Transfer in HgTe Nanoplatelet-Quantum Dot Heterostructures through High-Speed Exciton Diffusion. *J. Phys. Chem. Lett.* **2023**, *14*, 9456–9463.

(22) Izquierdo, E.; Dufour, M.; Chu, A.; Livache, C.; Martinez, B.; Amelot, D.; Patriarche, G.; Lequeux, N.; Lhuillier, E.; Ithurria, S. Coupled HgSe Colloidal Quantum Wells through a Tunable Barrier: A Strategy To Uncouple Optical and Transport Band Gap. *Chem. Mater.* **2018**, *30*, 4065–4072.

(23) Keuleyan, S.; Lhuillier, E.; Guyot-Sionnest, P. Synthesis of Colloidal HgTe Quantum Dots for Narrow Mid-IR Emission and Detection. *J. Am. Chem. Soc.* **2011**, *133*, 16422–16424.

(24) Rurack, K.; Spieles, M. Fluorescence Quantum Yields of a Series of Red and Near-Infrared Dyes Emitting at 600–1000 Nm. *Anal. Chem.* **2011**, *83*, 1232–1242.

(25) Hoshi, R.; Suzuki, K.; Hasebe, N.; Yoshihara, T.; Tobita, S. Absolute Quantum Yield Measurements of Near-Infrared Emission with Correction for Solvent Absorption. *Anal. Chem.* **2020**, *92*, 607−611.

(26) Atallah, T. L.; Sica, A. V.; Shin, A. J.; Friedman, H. C.; Kahrobai, Y. K.; Caram, J. R. Decay-Associated Fourier Spectroscopy: Visible to Shortwave Infrared Time-Resolved Photoluminescence Spectra. *J. Phys. Chem. A* **2019**, *123*, 6792−6798.

(27) Shen, G.; Chen, M.; Guyot-Sionnest, P. Synthesis of Nonaggregating HgTe Colloidal Quantum Dots and the Emergence of Air-Stable n-Doping. *J. Phys. Chem. Lett.* **2017**, *8*, 2224−2228.

(28) Yang, J.; Hu, H.; Lv, Y.; Yuan, M.; Wang, B.; He, Z.; Chen, S.; Wang, Y.; Hu, Z.; Yu, M.; et al. Ligand-Engineered HgTe Colloidal Quantum Dot Solids for Infrared Photodetectors. *Nano Lett.* **2022**, *22*, 3465−3472.

(29) Talapin, D. V.; Rogach, A. L.; Shevchenko, E. V.; Kornowski, A.; Haase, M.; Weller, H. Dynamic Distribution of Growth Rates within the Ensembles of Colloidal II−VI and III−V Semiconductor Nanocrystals as a Factor Governing Their Photoluminescence Efficiency. *J. Am. Chem. Soc.* **2002**, *124*, 5782−5790.

(30) Patterson, A. L. The Scherrer Formula for X-Ray Particle Size Determination. *Phys. Rev.* **1939**, *56*, 978−982.

(31) Vorokh, A. S. Scherrer Formula: Estimation of Error in Determining Small Nanoparticle Size. *Nanosyst.: phys., Chem., Math.* **2018**, *9*, 364−369.

(32) Kershaw, S. V.; Yiu, W. K.; Sergeev, A.; Rogach, A. L. Development of Synthetic Methods to Grow Long-Wavelength Infrared-Emitting HgTe Quantum Dots in Dimethylformamide. *Chem. Mater.* **2020**, *32*, 3930−3943.

(33) Kovalenko, M. V.; Kaufmann, E.; Pachinger, D.; Roither, J.; Huber, M.; Stangl, J.; Hesser, G.; Schäffler, F.; Heiss, W. Colloidal HgTe Nanocrystals with Widely Tunable Narrow Band Gap Energies: From Telecommunications to Molecular Vibrations. *J. Am. Chem. Soc.* **2006**, *128*, 3516−3517.

(34) Lhuillier, E.; Keuleyan, S.; Guyot-Sionnest, P. Optical Properties of HgTe Colloidal Quantum Dots. *Nanotechnology* **2012**, *23*, 175705.

(35) Keuleyan, S. E.; Guyot-Sionnest, P.; Delerue, C.; Allan, G. Mercury Telluride Colloidal Quantum Dots: Electronic Structure, Size-Dependent Spectra, and Photocurrent Detection up to 12 Mm. *ACS Nano.* **2014**, *8*, 8676−8682.

(36) Piepenbrock, M.-O. M.; Stirner, T.; Kelly, S. M.; O'Neill, M. A Low-Temperature Synthesis for Organically Soluble HgTe Nanocrystals Exhibiting Near-Infrared Photoluminescence and Quantum Confinement. *J. Am. Chem. Soc.* **2006**, *128*, 7087−7090.

(37) Xu, H.; Hou, Y.; Zhang, H. CdTe Magic-Sized Clusters and the Use as Building Blocks for Assembling Two-Dimensional Nanoplatelets. *J. Nanopart. Res.* **2017**, *19*, 189.

(38) Chen, M.; Luan, C.; Zhang, M.; Rowell, N.; Willis, M.; Zhang, C.; Wang, S.; Zhu, X.; Fan, H.; Huang, W.; et al. Evolution of CdTe Magic-Size Clusters with Single Absorption Doublet Assisted by Adding Small Molecules during Prenucleation. *J. Phys. Chem. Lett.* **2020**, *11*, 2230−2240.

(39) Luan, C.; Tang, J.; Rowell, N.; Zhang, M.; Huang, W.; Fan, H.; Yu, K. Four Types of CdTe Magic-Size Clusters from One Prenucleation Stage Sample at Room Temperature. *J. Phys. Chem. Lett.* **2019**, *10*, 4345−4353.

(40) Kudera, S.; Zanella, M.; Giannini, C.; Rizzo, A.; Li, Y.; Gigli, G.; Cingolani, R.; Ciccarella, G.; Spahl, W.; Parak, W. J.; et al. Sequential Growth of Magic-Size CdSe Nanocrystals. *Adv. Mater.* **2007**, *19*, 548−552.

(41) Harrell, S. M.; McBride, J. R.; Rosenthal, S. J. Synthesis of Ultrasmall and Magic-Sized CdSe Nanocrystals. *Chem. Mater.* **2013**, *25*, 1199−1210.

(42) Keuleyan, S.; Kohler, J.; Guyot-Sionnest, P. Photoluminescence of Mid-Infrared HgTe Colloidal Quantum Dots. *J. Phys. Chem. C* **2014**, *118*, 2749−2753.

(43) Xie, S.; Zhu, H.; Li, M.; Bulović, V. Voltage-Controlled Reversible Modulation of Colloidal Quantum Dot Thin Film Photoluminescence. *Appl. Phys. Lett.* **2022**, *120*, 211104.

(44) Zheng, C.; Bi, C.; Huang, F.; Binks, D.; Tian, J. Stable and Strong Emission $CsPbBr_3$ Quantum Dots by Surface Engineering for High-Performance Optoelectronic Films. *ACS Appl. Mater. Interfaces* **2019**, *11*, 25410−25416.

(45) Bertram, S. N.; Spokoyny, B.; Franke, D.; Caram, J. R.; Yoo, J. J.; Murphy, R. P.; Grein, M. E.; Bawendi, M. G. Single Nanocrystal Spectroscopy of Shortwave Infrared Emitters. *ACS Nano* **2019**, *13*, 1042−1049.

(46) Hu, Z.; Kim, Y.; Krishnamurthy, S.; Avdeev, I. D.; Nestoklon, M. O.; Singh, A.; Malko, A. V.; Goupalov, S. V.; Hollingsworth, J. A.; Htoon, H. Intrinsic Exciton Photophysics of PbS Quantum Dots Revealed by Low-Temperature Single Nanocrystal Spectroscopy. *Nano Lett.* **2019**, *19*, 8519−8525.

(47) Correa, R. E.; Dauler, E. A.; Nair, G.; Pan, S. H.; Rosenberg, D.; Kerman, A. J.; Molnar, R. J.; Hu, X.; Marsili, F.; Anant.; et al. Single Photon Counting from Individual Nanocrystals in the Infrared. *Nano Lett.* **2012**, *12*, 2953−2958.

(48) Bischof, T. S.; Correa, R. E.; Rosenberg, D.; Dauler, E. A.; Bawendi, M. G. Measurement of Emission Lifetime Dynamics and Biexciton Emission Quantum Yield of Individual InAs Colloidal Nanocrystals. *Nano Lett.* **2014**, *14*, 6787−6791.

(49) Caram, J. R.; Bertram, S. N.; Utzat, H.; Hess, W. R.; Carr, J. A.; Bischof, T. S.; Beyler, A. P.; Wilson, M. W. B.; Bawendi, M. G. PbS Nanocrystal Emission Is Governed by Multiple Emissive States. *Nano Lett.* **2016**, *16*, 6070−6077.

(50) Peterson, J. J.; Krauss, T. D. Fluorescence Spectroscopy of Single Lead Sulfide Quantum Dots. *Nano Lett.* **2006**, *6*, 510−514.

(51) Whitham, P. J.; Marchioro, A.; Knowles, K. E.; Kilburn, T. B.; Reid, P. J.; Gamelin, D. R. Single-Particle Photoluminescence Spectra, Blinking, and Delayed Luminescence of Colloidal CuInS2 Nanocrystals. *J. Phys. Chem. C* **2016**, *120*, 17136−17142.

(52) Nirmal, M.; Dabbousi, B. O.; Bawendi, M. G.; Macklin, J. J.; Trautman, J. K.; Harris, T. D.; Brus, L. E. Fluorescence Intermittency in Single Cadmium Selenide Nanocrystals. *Nature* **1996**, *383*, 802−804.

(53) Cordones, A. A.; Leone, S. R. Mechanisms for Charge Trapping in Single Semiconductor Nanocrystals Probed by Fluorescence Blinking. *Chem. Soc. Rev.* **2013**, *42*, 3209.

(54) Yuan, G.; Gómez, D. E.; Kirkwood, N.; Boldt, K.; Mulvaney, P. Two Mechanisms Determine Quantum Dot Blinking. *ACS Nano.* **2018**, *12*, 3397−3405.

(55) Frantsuzov, P. A.; Volkán-Kacsó, S.; Jankó, B. Model of Fluorescence Intermittency of Single Colloidal Semiconductor Quantum Dots Using Multiple Recombination Centers. *Phys. Rev. Lett.* **2009**, *103*, 207402.

(56) Efros, A. L.; Nesbitt, D. J. Origin and Control of Blinking in Quantum Dots. *Nat. Nanotechnol.* **2016**, *11*, 661−671.

(57) Ahmed, T.; Seth, S.; Samanta, A. Mechanistic Investigation of the Defect Activity Contributing to the Photoluminescence Blinking of CsPbBr3 Perovskite Nanocrystals. *ACS Nano.* **2019**, *13*, 13537−13544.

(58) Hines, M. A.; Scholes, G. D. Colloidal PbS Nanocrystals with Size-Tunable Near-Infrared Emission: Observation of Post-Synthesis Self-Narrowing of the Particle Size Distribution. *Adv. Mater.* **2003**, *15*, 1844−1849.

(59) Wise, F. W. Lead Salt Quantum Dots: The Limit of Strong Quantum Confinement. *Acc. Chem. Res.* **2000**, *33*, 773−780.

(60) Du, H.; Chen, C.; Krishnan, R.; Krauss, T. D.; Harbold, J. M.; Wise, F. W.; Thomas, M. G.; Silcox, J. Optical Properties of Colloidal PbSe Nanocrystals. *Nano Lett.* **2002**, *2*, 1321−1324.

(61) Joo, J.; Pietryga, J. M.; McGuire, J. A.; Jeon, S.-H.; Williams, D. J.; Wang, H.-L.; Klimov, V. I. A Reduction Pathway in the Synthesis of PbSe Nanocrystal Quantum Dots. *J. Am. Chem. Soc.* **2009**, *131*, 10620−10628.

(62) Yu, W. W.; Falkner, J. C.; Shih, B. S.; Colvin, V. L. Preparation and Characterization of Monodisperse PbSe Semiconductor Nano-

crystals in a Noncoordinating Solvent. *Chem. Mater.* **2004**, *16*, 3318−3322.

(63) Moreels, I.; Justo, Y.; De Geyter, B.; Haustraete, K.; Martins, J. C.; Hens, Z. Size-Tunable, Bright, and Stable PbS Quantum Dots: A Surface Chemistry Study. *ACS Nano.* **2011**, *5*, 2004−2012.

(64) Abel, K. A.; Shan, J.; Boyer, J.-C.; Harris, F.; van Veggel, F. C. J. M. Highly Photoluminescent PbS Nanocrystals: The Beneficial Effect of Trioctylphosphine. *Chem. Mater.* **2008**, *20*, 3794−3796.

(65) Liu, H.; Zhong, H.; Zheng, F.; Xie, Y.; Li, D.; Wu, D.; Zhou, Z.; Sun, X.-W.; Wang, K. Near-Infrared Lead Chalcogenide Quantum Dots: Synthesis and Applications in Light Emitting Diodes. *Chinese Phys. B* **2019**, *28*, 128504.

(66) Aharoni, A.; Mokari, T.; Popov, I.; Banin, U. Synthesis of InAs/CdSe/ZnSe Core/Shell1/Shell2 Structures with Bright and Stable Near-Infrared Fluorescence. *J. Am. Chem. Soc.* **2006**, *128*, 257−264.

(67) Gustafsson, O.; Karim, A.; Berggren, J.; Wang, Q.; Reuterskiöld-Hedlund, C.; Ernerheim-Jokumsen, C.; Soldemo, M.; Weissenrieder, J.; Persson, S.; Almqvist, S.; et al. Photoluminescence and Photoresponse from InSb/InAs-Based Quantum Dot Structures. *Opt. Express* **2012**, *20*, 21264−21271.

(68) De Trizio, L.; Manna, L.; Di Stasio, F. Indium Arsenide Quantum Dots: An Alternative to Lead-Based Infrared Emitting Nanomaterials. *Chem. Soc. Rev.* **2022**, *51*, 9861−9881.

(69) Killilea, N.; Wu, M.; Sytnyk, M.; Yousefi Amin, A. A.; Mashkov, O.; Spiecker, E.; Heiss, W. Pushing PbS/Metal-Halide-Perovskite Core/Epitaxial-Ligand-Shell Nanocrystal Photodetectors beyond 3 Mm Wavelength. *Adv. Funct. Mater.* **2019**, *29*, 1807964.

(70) Cheng, C.; Li, J.; Cheng, X. Photoluminescence Lifetime and Absorption Spectrum of PbS Nanocrystal Quantum Dots. *J. Lumin.* **2017**, *188*, 252−257.

(71) Stewart, J. T.; Padilha, L. A.; Qazilbash, M. M.; Pietryga, J. M.; Midgett, A. G.; Luther, J. M.; Beard, M. C.; Nozik, A. J.; Klimov, V. I. Comparison of Carrier Multiplication Yields in PbS and PbSe Nanocrystals: The Role of Competing Energy-Loss Processes. *Nano Lett.* **2012**, *12*, 622−628.

(72) Langford, N. J.; Ferner, R. E. Toxicity of Mercury. *J. Hum. Hypertens* **1999**, *13*, 651−656.

(73) Gréboval, C.; Chu, A.; Magalhaes, D. V.; Ramade, J.; Qu, J.; Rastogi, P.; Khalili, A.; Chee, S.-S.; Aubin, H.; Vincent, G.; et al. Ferroelectric Gating of Narrow Band-Gap Nanocrystal Arrays with Enhanced Light−Matter Coupling. *ACS Photonics* **2021**, *8*, 259−268.

(74) Chee, S.-S.; Gréboval, C.; Magalhaes, D. V.; Ramade, J.; Chu, A.; Qu, J.; Rastogi, P.; Khalili, A.; Dang, T. H.; Dabard, C.; et al. Correlating Structure and Detection Properties in HgTe Nanocrystal Films. *Nano Lett.* **2021**, *21*, 4145−4151.

(75) Cui, J.; Beyler, A. P.; Coropceanu, I.; Cleary, L.; Avila, T. R.; Chen, Y.; Cordero, J. M.; Heathcote, S. L.; Harris, D. K.; Chen, O.; et al. Evolution of the Single-Nanocrystal Photoluminescence Linewidth with Size and Shell: Implications for Exciton−Phonon Coupling and the Optimization of Spectral Linewidths. *Nano Lett.* **2016**, *16*, 289−296.

(76) Norris, D. J.; Efros, A. L.; Rosen, M.; Bawendi, M. G. Size Dependence of Exciton Fine Structure in CdSe Quantum Dots. *Phys. Rev. B* **1996**, *53*, 16347−16354.

(77) Kang, I.; Wise, F. W. Electronic Structure and Optical Properties of PbS and PbSe Quantum Dots. *J. Opt. Soc. Am. B* **1997**, *14*, 1632−1646.

(78) Farrell, R. E.; Germida, J. J.; Huang, P. M. Biotoxicity of Mercury as Influenced by Mercury(II) Speciation. *Appl. Environ. Microbiol.* **1990**, *56*, 3006−3016.

(79) National Center for Biotechnology Information. *PubChem Compound Summary For CID 43835023, Mercury(2+) Acetate.* PubChem. 2004. https://pubchem.ncbi.nlm.nih.gov/compound/Mercury_2_-acetate.

(80) National Center for Biotechnology Information. *PubChem Compound Summary For CID 24085, Mercuric Chloride.* PubChem. 2004. https://pubchem.ncbi.nlm.nih.gov/compound/Mercuric-Chloride.

(81) Frenette, L. C.; Krauss, T. D. Uncovering Active Precursors in Colloidal Quantum Dot Synthesis. *Nat. Commun.* **2017**, *8*, 2082.